

## Radiolabeled Phenethylguanidines: Novel Imaging Agents for Cardiac Sympathetic Neurons and Adrenergic Tumors

David M. Raffel,\* Yong-Woon Jung, David L. Gildersleeve, Phillip S. Sherman, James J. Moskwa, Louis J. Tluczek, and Wei Chen

Division of Nuclear Medicine, Department of Radiology, 3480 Kresge III Building, University of Michigan Medical School, Ann Arbor, Michigan 48109

Received December 6, 2006

The norepinephrine transporter (NET) substrates [ $^{123}\text{I}$ ]-*m*-iodobenzylguanidine (MIBG) and [ $^{11}\text{C}$ ]-*m*-hydroxyephedrine (HED) are used as markers of cardiac sympathetic neurons and adrenergic tumors (pheochromocytoma, neuroblastoma). However, their rapid NET transport rates limit their ability to provide accurate measurements of cardiac nerve density. [ $^{11}\text{C}$ ]Phenethylguanidine ([ $^{11}\text{C}$ ]**1a**) and 12 analogues ([ $^{11}\text{C}$ ]-**1b–m**) were synthesized and evaluated as radiotracers with improved kinetics for quantifying cardiac nerve density. In isolated rat hearts, neuronal uptake rates of [ $^{11}\text{C}$ ]**1a–m** ranged from 0.24 to 1.96 mL min $^{-1}$  (g wet wt) $^{-1}$ , and six compounds had extremely long neuronal retention times (clearance  $T_{1/2} > 20$  h) due to efficient vesicular storage. Positron emission tomography (PET) studies in nonhuman primates with [ $^{11}\text{C}$ ]-**1e**, *N*-[ $^{11}\text{C}$ ]guanyl-*m*-octopamine, which has a slow NET transport rate, showed improved myocardial kinetics compared to HED. Compound [ $^{11}\text{C}$ ]**1c**, [ $^{11}\text{C}$ ]-*p*-hydroxyphenethylguanidine, which has a rapid NET transport rate, avidly accumulated into rat pheochromocytoma xenograft tumors in mice. These encouraging findings demonstrate that radiolabeled phenethylguanidines deserve further investigation as radiotracers of cardiac sympathetic innervation and adrenergic tumors.

### Introduction

Radioiodinated *m*-iodobenzylguanidine (MIBG, Figure 1) was originally developed by Wieland and co-workers $^{1-3}$  as a radiotracer for scintigraphic imaging studies of adrenergic tumors such as neuroblastoma and pheochromocytoma. As a structural analogue of the neurotransmitter norepinephrine, MIBG concentrates in adrenergic tumors through active transport by the norepinephrine transporter (NET), which is richly expressed in the cell membranes of these tumors. $^{4-6}$  In addition to its successful application as a marker of adrenergic tumors, MIBG has proven to be very useful for scintigraphic imaging studies of cardiac sympathetic innervation. $^{7,8}$  MIBG is rapidly transported into cardiac sympathetic neurons by NET populations localized on the varicosities of terminal nerve axons. $^9$  Following uptake into the neuronal axoplasm, MIBG is transported into norepinephrine storage vesicles by the second isoform of the vesicular monoamine transporter (VMAT2), $^{7,10}$  the isoform expressed in peripheral sympathetic nerve terminals. $^{11}$

With the advent of positron emission tomography (PET), several radiotracers labeled with positron-emitting radioisotopes were developed for PET studies of cardiac sympathetic innervation and adrenergic tumors. Early examples included the fluorine-18-labeled compounds 6-[ $^{18}\text{F}$ ]fluorometaraminol $^{12}$  and 6-[ $^{18}\text{F}$ ]fluorodopamine. $^{13}$  Following these were several carbon-11-labeled compounds, most in the form of *N*-[ $^{11}\text{C}$ ]methylphenethylamines, including [ $^{11}\text{C}$ ]-*m*-hydroxyephedrine ([ $^{11}\text{C}$ ]HED, Figure 1), $^{14}$  [ $^{11}\text{C}$ ]epinephrine ([ $^{11}\text{C}$ ]EPI, Figure 1), $^{15}$  and [ $^{11}\text{C}$ ]-phenylephrine. $^{16}$  Positron-emitter-labeled analogues of MIBG have also been synthesized, including *m*-[ $^{76}\text{Br}$ ]bromobenzylguanidine $^{17}$  and *p*-[ $^{18}\text{F}$ ]fluorobenzylguanidine. $^{18}$  While all of these compounds avidly localize in cardiac sympathetic neurons, there are significant differences in their neuronal handling in

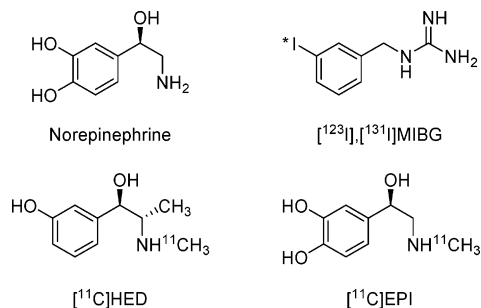


**Figure 1.** Structures of norepinephrine and some clinically used sympathetic nerve imaging agents.

terms of NET transport rates, vulnerability to intraneuronal enzyme metabolism, efficiency of vesicular storage, and diffusion rates from neurons. $^{19}$

[ $^{11}\text{C}$ ]HED has been used extensively to study changes in cardiac sympathetic innervation in diabetic autonomic neuropathy, congestive heart failure, myocardial infarction, cardiac arrhythmias, and heart transplant patients. $^{20}$  The ability to assess the integrity of cardiac sympathetic innervation with radiotracers like [ $^{11}\text{C}$ ]HED provides clinicians with valuable insights into a critical component of cardiac function. The physiologic information gained from these studies complements more traditional nuclear cardiology assessments of myocardial perfusion and myocardial viability.

While studies with the current generation of sympathetic nerve radiotracers have provided a wealth of information, all of these tracers share one common drawback: their uptake rates into cardiac sympathetic neurons are too rapid to allow for robust and reliable compartmental modeling of their kinetics. The inability to use kinetic modeling methods limits the quantitative information that can be garnered from clinical studies with these tracers. This situation is illustrated for [ $^{11}\text{C}$ ]HED in Figure 2A. Following its delivery from plasma into the extracellular space ( $K_1$ ), [ $^{11}\text{C}$ ]HED is very rapidly taken up into sympathetic

\* Corresponding author: telephone (734) 936-0725; fax (734) 764-0288; e-mail raffel@umich.edu.

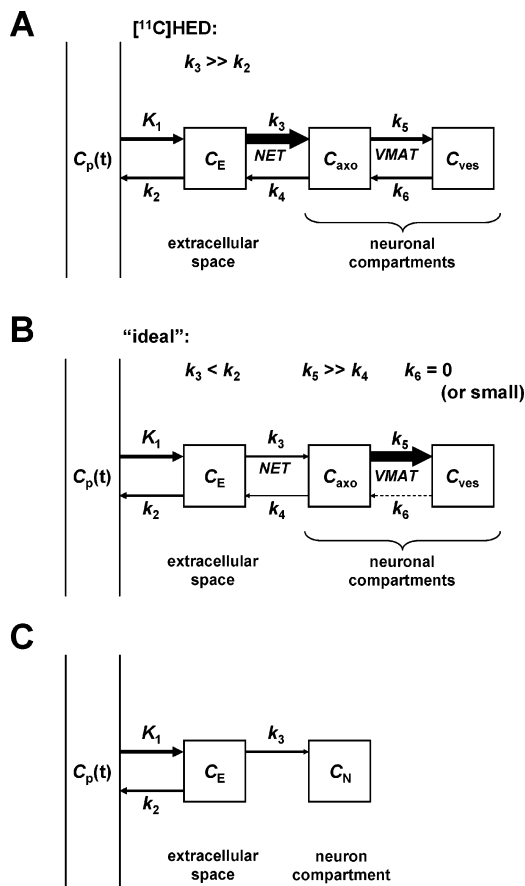


**Figure 2.** (A) Comprehensive compartmental model of  $[^{11}\text{C}]\text{HED}$  kinetics in the heart. Arrow thicknesses indicate relative magnitudes of rate constants.  $K_1$  has units of milliliters per minute per gram; all other rate constants have units of  $\text{minute}^{-1}$ .  $C_p$  = concentration in plasma;  $C_E$  = concentration in extracellular space;  $C_{axo}$  = concentration in neuronal axoplasm;  $C_{ves}$  = concentration in vesicles; NET = norepinephrine transporter; VMAT = vesicular monoamine transporter. (B) Comprehensive compartmental model of a tracer with "ideal" kinetic properties for kinetic modeling. (C) Simplified compartmental model that could be used to analyze the myocardial kinetics of a PET tracer possessing the ideal kinetic properties shown in panel B.

neurons by NET transport ( $k_3$ ). The rapid neuronal uptake of  $[^{11}\text{C}]\text{HED}$  by NET transport ( $k_3$ ) is much faster than clearance of the tracer from the extracellular space back to plasma ( $k_2$ ), such that  $k_3 \gg k_2$ . Because neuronal uptake is much faster than clearance back to plasma, uptake of  $[^{11}\text{C}]\text{HED}$  into cardiac sympathetic neurons is rate-limited by delivery of the tracer from plasma to interstitium ( $K_1$ ) rather than by NET transport ( $k_3$ ). While it is evident from the shape of the myocardial kinetics of  $[^{11}\text{C}]\text{HED}$  that its neuronal uptake by NET transport is a fast process, it is so fast that there is insufficient information in the measured kinetics to precisely estimate the value of  $k_3$  by kinetic modeling methods. This forces the use of semiquantitative measurements of tracer retention instead of the more quantitative information provided by tracer kinetic modeling.<sup>19,20</sup> However, since neuronal uptake by NET transport ( $k_3$ ) is much faster than clearance from interstitium back into plasma ( $k_2$ ),  $[^{11}\text{C}]\text{HED}$  retention measurements are insensitive to low-to-moderate losses in NET density (i.e., nerve density) and decline only in myocardial regions in which nerve losses are severe.<sup>21</sup> Thus, the rapid neuronal uptake rate of  $[^{11}\text{C}]\text{HED}$  not only prevents successful tracer kinetic modeling of its myocardial kinetics but also tends to make measurements of its cardiac retention insensitive to low-to-moderate levels of nerve loss.

We hypothesized that this roadblock to accurate quantification could be overcome by developing a new radiotracer with inherently superior kinetic properties (Figure 2B). Specifically we hypothesized that a cardiac sympathetic nerve tracer would need to possess two kinetic properties to be ideal for quantitative analyses: (1) a slower neuronal uptake rate than current tracers such as  $[^{11}\text{C}]\text{HED}$  and (2) a very long neuronal retention time, through trapping inside norepinephrine storage vesicles. The first criterion makes the neuronal uptake rate of the tracer rate-limited by NET transport ( $k_3$ ) rather than by delivery from plasma to interstitium ( $K_1$ ), by establishing conditions in which NET transport is slower than clearance from interstitium back into plasma ( $k_3 < k_2$ ). A slower NET transport rate would allow some clearance of the tracer from tissue back into plasma after its initial extraction, greatly improving the ability of compartmental modeling techniques to make an accurate estimate of the neuronal uptake rate  $k_3$  from the observed myocardial kinetics. In addition, it would make measurements of tracer retention more sensitive to early losses in nerve density, allowing earlier detection of cardiac denervation in diseases. The second criterion has two purposes. First, since NET transport of the new tracer would be slower than for previous tracers, if the tracer was also efficiently trapped intraneuronally this would maximize the amount of radioactivity retained in the neurons, increasing image quality and providing better counting statistics for kinetic modeling efforts. Second, complete trapping of the tracer in the neuron following its neuronal uptake permits a simplification in the compartmental model structure, reducing the number of model parameters that need to be estimated from the kinetic data. This is important for PET studies where kinetic models with more than three or four rate constants are unfeasible. In this case, a "trapped" neuronal tracer could be analyzed with the simplified compartmental model shown in Figure 2C. The estimated value of  $k_3$  in this simplified model would be a direct estimate of the neuronal transport rate of the radiotracer. Since neuronal transport rate by NET is highly sensitive to changes in nerve density, accurate estimates of this rate constant would effectively provide quantitative regional estimates of cardiac sympathetic nerve density. Such a tracer would represent a major advance in this branch of nuclear cardiology since it could be used to provide truly quantitative measures of regional nerve density. These measures would be more accurate and sensitive than the semiquantitative measures of tracer retention used for the current generation of sympathetic nerve tracers.

Since vesicular storage is the mechanism we chose to exploit as a means of trapping a kinetically "ideal" radiotracer inside sympathetic neurons, we decided to investigate radiolabeled phenethylguanidines as a potential class of compounds with high vesicular retention. Many phenethylguanidines are known to be potent depletors of cardiac norepinephrine stores in vivo, due to their avid uptake and retention inside norepinephrine storage vesicles.<sup>22,23</sup> In addition, phenethylguanidines have been shown to be more potent depletors of cardiac norepinephrine stores than benzylguanidines.<sup>24</sup> Although radiolabeled benzylguanidines such as  $[^{123}\text{I}]\text{MIBG}$  have been extensively studied as sympathetic nerve imaging agents, very little work has been done with radiolabeled phenethylguanidines. With these points in mind, we synthesized and evaluated a series of  $[^{11}\text{C}]\text{phenethylguanidines}$  as potentially optimal imaging agents for PET studies of cardiac innervation (Figure 3).

Although these studies employed carbon-11 as the radiolabel, some of the phenethylguanidine structures evaluated included compounds with a ring fluoro or iodo group, with the idea that

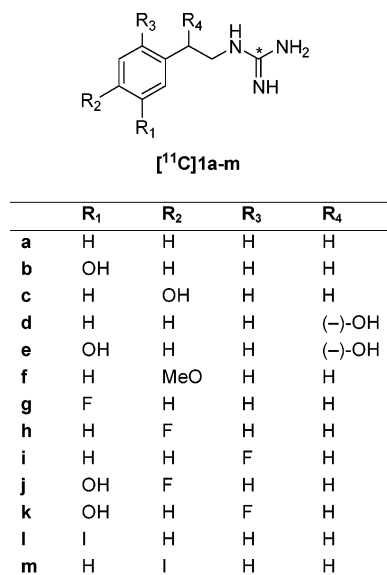


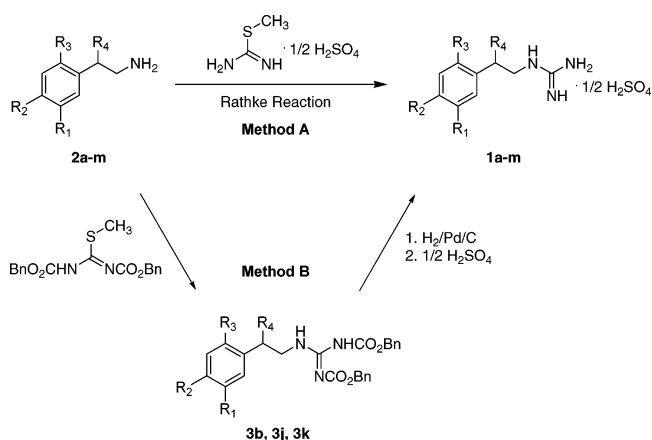
**Figure 3.** General structure of [<sup>11</sup>C]phenethylguanidines and compounds synthesized.

a successful compound could ultimately be synthesized with its corresponding radioisotope [i.e., replacing ring fluoro group with fluorine-18 for PET imaging or ring iodo group with iodine-123 for single photon emission computed tomography (SPECT) imaging]. While it is possible that changing the radiolabel from carbon-11 in the guanidine group of the side chain to a ring fluorine-18 or iodine-123 would lead to changes in the specific radiolabeled metabolites formed during an imaging study, we believe the *in vivo* kinetics of the <sup>18</sup>F- or <sup>123</sup>I-labeled parent compounds would be very similar to those seen for their corresponding <sup>11</sup>C-labeled phenethylguanidines.

For cardiac PET imaging studies, carbon-11 and fluorine-18 are both good choices for the radiolabel. Carbon-11 may offer some advantages in terms of being able to inject 2–3 times more activity into a patient due to more favorable radiation dosimetry over fluorine-18. This provides higher tissue and blood concentrations of the tracer early in the study, when the kinetics of the tracer are changing most rapidly. In addition, the radiosynthetic methods to prepare the carbon-11 compound are much simpler and faster than those required to prepare a fluorine-18 compound. However, the use of carbon-11 requires that a PET center have an onsite cyclotron and staff to prepare the radiopharmaceutical. A successful fluorine-18-labeled compound could be prepared by commercial vendors and distributed to stand-alone PET centers for cardiac and cancer imaging studies, much as the glucose analogue 2-[<sup>18</sup>F]fluoro-2-deoxyglucose (FDG) is distributed today. In terms of the kinetics of these tracers, however, it should be emphasized that we are not attempting to measure the overall clearance rates of these compounds from the heart, so it is not necessary to use a radiolabel with a longer half-life than carbon-11. The main goal of developing a radiotracer with a slower NET transport rate and very long neuronal retention time is to bestow the tracer with kinetic properties that allow its neuronal uptake rate  $k_3$  to be accurately estimated from the myocardial kinetics measured during a 60 min PET study.

Finally, in addition to the main goal of developing an optimal PET tracer for quantitative studies of cardiac sympathetic innervation, a secondary goal was to test the ability of [<sup>11</sup>C]phenethylguanidines to act as imaging agents for localization of adrenergic tumors.

### Scheme 1

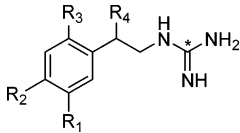


### Results and Discussion

**Chemistry.** Phenethylguanidines **1a–m** were synthesized for HPLC standards and *in vitro* studies (Scheme 1). Most of the primary amine precursors **2a–m** were available commercially, but 4-fluoro- and 6-fluoro-3-hydroxyphenethylamines (**2j** and **2k**) were prepared in multiple steps from 4-fluoro- or 6-fluoro-3-methoxybenzaldehyde utilizing previously published methods.<sup>25</sup> Two established methods were used to prepare **1a–m** (Scheme 1). Method A, the Rathke reaction,<sup>26,27</sup> involves nucleophilic attack by the phenethylamine precursor on the amidine derivative 2-methyl-2-thiopseudourea to yield the phenethylguanidine, which was subsequently purified by recrystallization. Method B is a two-step reaction: condensation of the phenethylamine precursor with 1,3-bis(benzyloxycarbonyl)-2-methyl-2-thiopseudourea<sup>28</sup> is followed by hydrogenolysis over Pd/C to afford the phenethylguanidine. Although the Rathke reaction is a straightforward one-step reaction, some phenethylguanidines could not be purified by recrystallization due to poor separation from the reactant 2-methyl-2-thiopseudourea and phenethylamine precursors. We successfully used the Rathke method to synthesize most compounds (**1a** and **1c–i**). Chemical yields were 32–93% and chemical purities were >98% after several recrystallizations from ethanol in water. Method B was used to synthesize the remaining phenethylguanidines (**1b**, **1j**, and **1k**). Chemical yields were 63–82% and chemical purities were >95%. Chemical purities were determined by high-performance liquid chromatography (HPLC) with UV detection (241 nm).

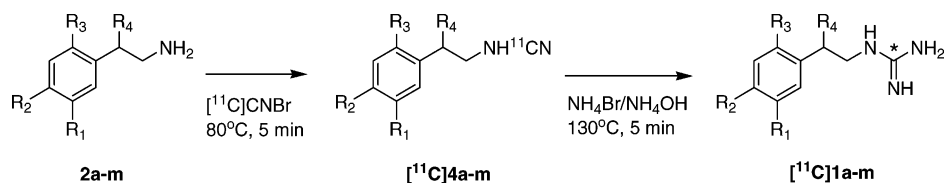
**Radiochemistry.** [<sup>11</sup>C]Phenethylguanidines ([<sup>11</sup>C]**1a–m**) were synthesized from [<sup>11</sup>C]CNBr by methods developed by Westergberg and Långström<sup>29</sup> with a few modifications (Scheme 2). The phenethylamine precursor (**2a–m**; 1.0–1.5 mg), as the free base or hydrochloride salt, dissolved in 0.25 mL of borate buffer (pH 8.0), was reacted with [<sup>11</sup>C]CNBr to produce the [<sup>11</sup>C]-cyanamide intermediate [<sup>11</sup>C]**4a–m**, followed by treatment with ammonia to yield [<sup>11</sup>C]**1a–m**. The product was purified by reversed-phase HPLC. Corrected radiochemical yields were 2.5–6% (relative to [<sup>11</sup>C]CO<sub>2</sub> produced), with specific activities of >500 Ci/mmol at end of synthesis (EOS). Radiochemical and chemical purities were >98%. For most compounds, 25–60 mCi of [<sup>11</sup>C]phenethylguanidine was obtained at EOS.

**Kinetic Studies in Isolated Rat Heart.** Uptake rates of [<sup>11</sup>C]**1a–m** into sympathetic neurons, as well as the ability of cardiac neurons to retain these compounds, were assessed by performing kinetic studies in an isolated working rat heart preparation. In all of these studies, the extraneuronal catecholamine uptake mechanism in the rat heart (“uptake-2”) was inhibited by adding

**Table 1.** Neuronal Uptake and Clearance Rates of [<sup>11</sup>C]Phenethylguanidines in Isolated Rat Heart<sup>a</sup>


compd	R <sub>1</sub>	R <sub>2</sub>	R <sub>3</sub>	R <sub>4</sub>	name	acronym	K <sub>up</sub> (mL min <sup>-1</sup> g <sup>-1</sup> )	major clearance T <sub>1/2</sub> (h)
[ <sup>11</sup> C] <b>1a</b>	H	H	H	H	[ <sup>11</sup> C]phenethylguanidine (PG)	PG	1.56	3.3
[ <sup>11</sup> C] <b>1b</b>	OH	H	H	H	[ <sup>11</sup> C]- <i>m</i> -hydroxy-PG	MHPG	1.96 ± 0.13	>102
[ <sup>11</sup> C] <b>1c</b>	H	OH	H	H	[ <sup>11</sup> C]- <i>p</i> -hydroxy-PG	PHPG	1.64 ± 0.15	>45
[ <sup>11</sup> C] <b>1d</b>	H	H	H	(-)-OH	[ <sup>11</sup> C]-(-)-β-hydroxy-PG	BHPG	0.42	22
[ <sup>11</sup> C] <b>1e</b>	OH	H	H	(-)-OH	<i>N</i> -[ <sup>11</sup> C]guanyl- <i>m</i> -octopamine	GMO	0.30 ± 0.02	>152
[ <sup>11</sup> C] <b>1f</b>	H	MeO	H	H	[ <sup>11</sup> C]- <i>p</i> -methoxy-PG	PMPG	0.73	2.3
[ <sup>11</sup> C] <b>1g</b>	F	H	H	H	[ <sup>11</sup> C]- <i>m</i> -fluoro-PG	MFPG	0.24	1.9
[ <sup>11</sup> C] <b>1h</b>	H	F	H	H	[ <sup>11</sup> C]- <i>p</i> -fluoro-PG	PFPG	0.63	4.4
[ <sup>11</sup> C] <b>1i</b>	H	H	F	H	[ <sup>11</sup> C]- <i>o</i> -fluoro-PG	OFPG	1.76	2.3
[ <sup>11</sup> C] <b>1j</b>	OH	F	H	H	[ <sup>11</sup> C]- <i>p</i> -fluoro- <i>m</i> -hydroxy-PG	4F-MHPG	0.72 ± 0.05	>73
[ <sup>11</sup> C] <b>1k</b>	OH	H	F	H	[ <sup>11</sup> C]- <i>o</i> -fluoro- <i>m</i> -hydroxy-PG	6F-MHPG	0.49 ± 0.07	>20
[ <sup>11</sup> C] <b>1l</b>	I	H	H	H	[ <sup>11</sup> C]- <i>m</i> -iodo-PG	MIPG	1.10	2.4
[ <sup>11</sup> C] <b>1m</b>	H	I	H	H	[ <sup>11</sup> C]- <i>p</i> -iodo-PG	PIPG	0.56	1.9

<sup>a</sup> For compounds with multiple determinations, K<sub>up</sub> data are mean ± standard deviation (SD) and T<sub>1/2</sub> is the fastest measured clearance rate for n = 5 independent determinations. Coefficients of variation (SD/mean) for these ranged from 7% to 14%. Single determination values can be expected to be within this range. Extraneuronal uptake (uptake-2) was inhibited in all studies by adding 54 μM corticosterone to the perfusate.

**Scheme 2**

54 μM corticosterone to all heart perfusion buffers.<sup>30</sup> Neuronal uptake rates (K<sub>up</sub>; milliliters per minute per gram wet weight) were measured by performing a 10 min infusion of the radiotracer at a constant perfusate concentration into the isolated heart. At the end of the constant infusion period, the heart was switched to normal perfusion buffer for 120 min to measure radiotracer clearance rates (expressed as a half-time, T<sub>1/2</sub>, in hours). Neuronal uptake rates for [<sup>11</sup>C]**1a–m** varied widely, ranging from 0.24 mL min<sup>-1</sup> (g wet wt)<sup>-1</sup> for [<sup>11</sup>C]**1g** to 1.96 mL min<sup>-1</sup> (g wet wt)<sup>-1</sup> for [<sup>11</sup>C]**1b** (Table 1). These are all slower than the previously measured neuronal uptake rates of 2.66 mL min<sup>-1</sup> (g wet wt)<sup>-1</sup> for [<sup>11</sup>C]HED<sup>31</sup> and 3.66 mL min<sup>-1</sup> (g wet wt)<sup>-1</sup> for [<sup>123</sup>I]MIBG.<sup>9</sup> However, some were faster than the reported rate of 0.66 mL min<sup>-1</sup> (g wet wt)<sup>-1</sup> for [<sup>11</sup>C]EPI,<sup>32</sup> suggesting that compounds with neuronal uptake rates lower than this value may be the ones best suited for kinetic modeling in cardiac PET studies. Clearance rates fell into one of two groups, those with relatively fast clearance (clearance T<sub>1/2</sub> = 1.9–4.4 h) and those with extremely long neuronal retention (clearance T<sub>1/2</sub> > 20 h). These clearance rates can be compared to values of 1.1 h for [<sup>11</sup>C]HED<sup>31</sup> and 1.9 h for [<sup>123</sup>I]MIBG,<sup>9</sup> while retention of [<sup>11</sup>C]EPI in the isolated rat heart also is extremely long.<sup>32</sup> Six of the 13 phenethylguanidine structures exhibited the desired kinetic property of a very long neuronal retention time (Figure 4A). These six compounds share a common structural feature of having at least one hydroxyl substitution in either the phenyl ring or the β-carbon of the side chain. In fact, from examination of Table 1 it can be seen that the six compounds with at least one hydroxyl substitution all had very long neuronal retention times, while the remaining compounds lacking a hydroxyl substitution had faster clearance rates. Thus it appears that a minimum structural requirement for long neuronal retention is a β-carbon or phenyl ring hydroxyl group substitution. It has been shown that phenethylamines must possess at least two hydroxyl groups to be tightly bound inside

the storage vesicles of cardiac sympathetic neurons.<sup>33</sup> Thus it appears that the highly polar *N*-[<sup>11</sup>C]guanyl group of these [<sup>11</sup>C]-phenethylguanidines is acting like a hydroxyl group in terms of contributing to high vesicular uptake and retention, such that the addition of a single hydroxyl group to the phenethylguanidine structure is sufficient to ensure prolonged vesicular retention.

The main effect of ring hydroxylation at the meta or para position was to extend neuronal retention times. For example, when [<sup>11</sup>C]**1b** and [<sup>11</sup>C]**1c** are compared to the unsubstituted reference compound [<sup>11</sup>C]**1a**, there were modest effects on neuronal uptake rate but neuronal retention times were greatly prolonged. Similarly, when [<sup>11</sup>C]**1d** is compared with its *m*-hydroxylated analogue [<sup>11</sup>C]**1e**, little difference in the neuronal uptake rates was seen but [<sup>11</sup>C]**1e** had a much longer retention time. Addition of a *m*-hydroxy group to [<sup>11</sup>C]**1h** and [<sup>11</sup>C]**1i** to form [<sup>11</sup>C]**1j** and [<sup>11</sup>C]**1k**, respectively, also led to greatly extended neuronal retention times. However, [<sup>11</sup>C]**1k** did have a significantly slower neuronal uptake rate than [<sup>11</sup>C]**1i**, so in some cases ring hydroxylation does appear to affect the neuronal uptake rate.

Ring fluoro substitutions affected both neuronal uptake rates and clearance rates. The neuronal uptake and clearance kinetics of the unsubstituted reference compound [<sup>11</sup>C]**1a** and its *o*-fluoro ([<sup>11</sup>C]**1i**), *p*-fluoro ([<sup>11</sup>C]**1h**), and *m*-fluoro ([<sup>11</sup>C]**1g**) analogues are shown in Figure 4B. While these compounds did not exhibit the desired long neuronal retention for cardiac applications, it is possible that one of these compounds, if labeled with fluorine-18, could be useful for detection of adrenergic tumors by PET. The radiolabeled benzylguanidine *p*-[<sup>18</sup>F]fluorobenzylguanidine ([<sup>18</sup>F]PFBG) has previously been shown to be capable of detecting pheochromocytomas with PET.<sup>34</sup> In the isolated rat heart, [<sup>18</sup>F]PFBG has a neuronal uptake rate of 1.2 mL min<sup>-1</sup> (g wet wt)<sup>-1</sup> and a clearance T<sub>1/2</sub> of 0.53 h.<sup>35</sup> Thus, the fluorine-18 analogue of compound [<sup>11</sup>C]**1i**, which has a faster neuronal

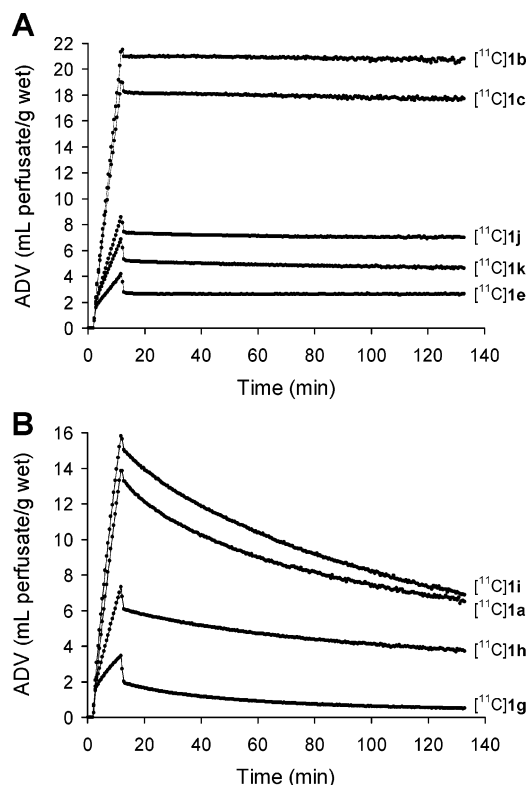


**Figure 4.** Neuronal uptake and clearance kinetics of [ $^{11}\text{C}$ ]phenethylguanidines in isolated rat heart. (A) Five of the six compounds that exhibited long neuronal retention times. For clarity, compound [ $^{11}\text{C}$ ]1d is not shown due to its similar kinetics with [ $^{11}\text{C}$ ]1k. (B) Unsubstituted reference compound [ $^{11}\text{C}$ ]1a and the three analogues with a single ring fluoro substitution.

uptake rate [ $1.76 \text{ mL min}^{-1} (\text{g wet wt})^{-1}$ ] and slower clearance rate ( $T_{1/2} = 2.3 \text{ h}$ ) than [ $^{18}\text{F}$ ]PFBG, could potentially be useful as a PET imaging agent for localizing adrenergic tumors.

The *m*-iodo ([ $^{11}\text{C}$ ]1l) and *p*-iodo ([ $^{11}\text{C}$ ]1m) compounds had slower neuronal uptake rates and faster clearance rates than the unsubstituted reference compound [ $^{11}\text{C}$ ]1a. Both compounds have neuronal uptake rates that are slower than the rate measured for the clinically used compound [ $^{123}\text{I}$ ]MIBG ( $3.66 \text{ mL min}^{-1} (\text{g wet wt})^{-1}$ ) but have clearance rates comparable to the 1.9 h value measured for [ $^{123}\text{I}$ ]MIBG.<sup>9</sup> The perfusate concentrations of [ $^{11}\text{C}$ ]1l and [ $^{11}\text{C}$ ]1m were  $<10 \text{ nM}$ , which is 5 times lower than the  $K_m$  for NET transport of [ $^{123}\text{I}$ ]MIBG ( $52 \text{ nM}$ ) in the isolated rat heart,<sup>36</sup> so we believe our measurements with these compounds can be directly compared to the reported values for [ $^{123}\text{I}$ ]MIBG without concerns of specific activity effects. The slower neuronal uptake rate of these iodophenethylguanidines may make their cardiac retention in human heart more sensitive to low-to-moderate degrees of cardiac denervation than [ $^{123}\text{I}$ ]MIBG, since their neuronal uptake is less likely to be rate-limited by delivery from plasma. Thus an  $^{123}\text{I}$ -labeled analogue of either compound [ $^{11}\text{C}$ ]1l or [ $^{11}\text{C}$ ]1m may prove to be clinically useful for assessing cardiac sympathetic innervation with SPECT imaging.

To verify that vesicular storage is the mechanism responsible for the prolonged neuronal retention of some [ $^{11}\text{C}$ ]phenethylguanidines, the neuronal uptake and retention of [ $^{11}\text{C}$ ]1c was measured in a heart isolated from a rat treated with the potent VMAT2 inhibitor reserpine ( $1 \text{ mg/kg}$  intraperitoneally, 3 h before heart isolation). Blocking vesicular uptake of [ $^{11}\text{C}$ ]1c with reserpine greatly reduced retention of the compound, both by reducing tracer accumulation into neurons during the constant infusion period and by accelerating the clearance rate during

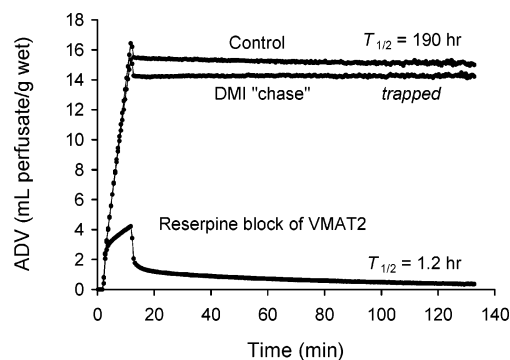


**Figure 5.** Kinetics of [ $^{11}\text{C}$ ]1c in isolated rat heart under (a) control conditions; (b) desipramine (DMI) chase to prevent neuronal reuptake during tracer clearance; and (c) reserpine block of vesicular storage.

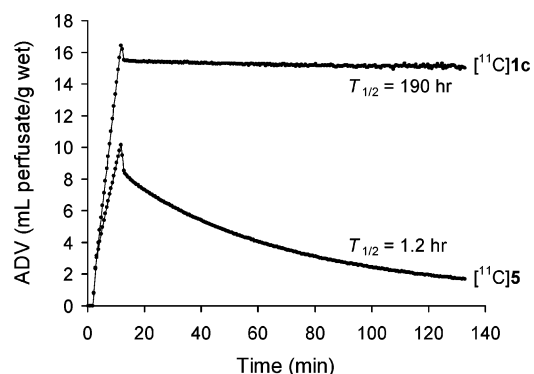


**Figure 6.** Kinetics of [ $^{11}\text{C}$ ]1c and its benzylguanidine analogue [ $^{11}\text{C}$ ]5 in isolated rat heart.

the washout phase of the study (Figure 5). Thus vesicular storage is a very important process that increases the tracer's neuronal distribution volume and prolongs tracer retention. To test whether significant leakage of [ $^{11}\text{C}$ ]1c occurs from vesicles and nerve terminals during the clearance phase of the study, with neuronal reuptake by NET as a potential mechanism for prolonging its neuronal retention, a pharmacological chase study was performed. The high-affinity NET inhibitor desipramine (DMI) was added to the heart perfusion buffer for the clearance phase of the study. As seen in Figure 5, DMI chase not only did not accelerate the clearance of [ $^{11}\text{C}$ ]1c from the nerves, consistent with the view that the compound remains largely sequestered inside storage vesicles, but instead prevented any measurable release of [ $^{11}\text{C}$ ]1c from the nerve terminals. The observation that DMI chase acted to completely abolish neuronal clearance suggests that the primary mechanism of [ $^{11}\text{C}$ ]1c clearance from nerves in the isolated rat heart is through NET transport acting in reverse, rather than through passive diffusion.

To test the hypothesis that [ $^{11}\text{C}$ ]phenethylguanidines are more avidly taken up and retained by storage vesicles than [ $^{11}\text{C}$ ]benzylguanidines, we prepared [ $^{11}\text{C}$ ]5, [ $^{11}\text{C}$ ]-*p*-hydroxybenzylguanidine (PHBG), the benzylguanidine analogue of compound [ $^{11}\text{C}$ ]1c. The kinetics of [ $^{11}\text{C}$ ]5 in the isolated rat heart are shown in Figure 6, in comparison with those of [ $^{11}\text{C}$ ]1c. [ $^{11}\text{C}$ ]5 had a slower neuronal uptake rate than [ $^{11}\text{C}$ ]1c [ $K_{up} = 0.93 \text{ mL min}^{-1} (\text{g wet wt})^{-1}$ ] and a much faster clearance time ( $T_{1/2} = 1.2 \text{ h}$ ). Although this finding is only for a single structural pair, the striking difference in the neuronal retention times of these two compounds suggests that some phenethylguanidines are better substrates for vesicular uptake by VMAT2 than their benzylguanidine analogues.

**Biodistribution Studies in Rats.** For the six [ $^{11}\text{C}$ ]phenethylguanidines that exhibited very long neuronal retention times

**Table 2.** Tissue Concentrations of  $^{11}\text{C}$ -Labeled Compounds at  $T = 30$  min in Rats<sup>a</sup>

compd	left ventricle	lung	liver	spleen	muscle	adrenal medulla	blood
[ $^{11}\text{C}$ ]HED	2.85 ± 0.42	0.40 ± 0.12	2.32 ± 0.25	1.31 ± 0.14	0.17 ± 0.02	0.72 ± 0.08	0.08 ± 0.01
[ $^{11}\text{C}$ ]EPI	2.14 ± 0.32	0.39 ± 0.05	1.95 ± 0.16	0.64 ± 0.02	0.22 ± 0.03	0.61 ± 0.18	0.13 ± 0.01
[ $^{11}\text{C}$ ]1b	2.28 ± 0.12	0.74 ± 0.15	0.89 ± 0.13	0.63 ± 0.16	0.07 ± 0.01	0.88 ± 0.15	0.07 ± 0.01
[ $^{11}\text{C}$ ]1c	3.30 ± 0.28	0.68 ± 0.16	0.84 ± 0.21	0.97 ± 0.06	0.14 ± 0.04	1.17 ± 0.16	0.16 ± 0.01
[ $^{11}\text{C}$ ]1d	1.91 ± 0.16	0.86 ± 0.11	3.91 ± 0.23	0.88 ± 0.07	0.10 ± 0.03	0.53 ± 0.07	0.09 ± 0.01
[ $^{11}\text{C}$ ]1e	1.17 ± 0.14	0.75 ± 0.10	2.71 ± 0.36	0.63 ± 0.10	0.07 ± 0.01	0.36 ± 0.06	0.14 ± 0.01
[ $^{11}\text{C}$ ]1j	1.77 ± 0.27	0.56 ± 0.15	1.22 ± 0.18	0.52 ± 0.10	0.07 ± 0.01	0.56 ± 0.21	0.08 ± 0.01
[ $^{11}\text{C}$ ]1k	1.01 ± 0.12	0.34 ± 0.06	0.92 ± 0.07	0.43 ± 0.12	0.06 ± 0.01	0.46 ± 0.07	0.07 ± 0.01

<sup>a</sup> Values are percent injected dose per gram; mean ± standard deviation of 5 determinations.

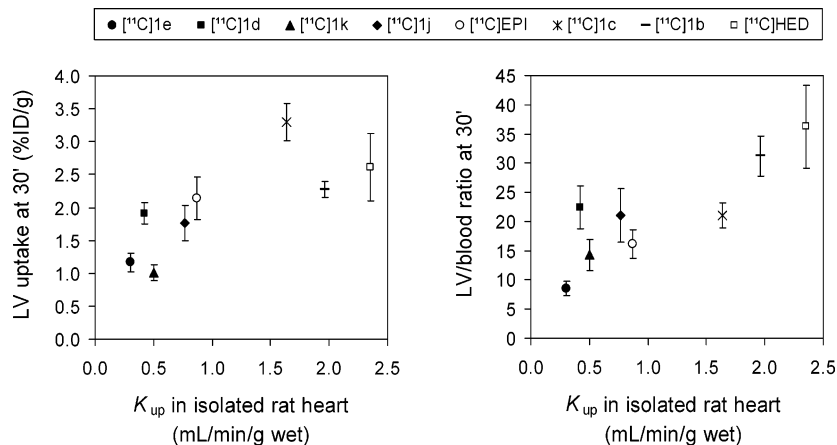


**Figure 7.** Relationship between in vivo uptake of compounds in rat left ventricle (LV) and neuronal uptake rates measured in isolated rat heart ( $K_{up}$ ).

in the isolated rat heart, in vivo biodistribution studies were performed in rats (Table 2). Tissue concentrations of the radiotracer were determined 30 min after intravenous injection and expressed as a percentage of the injected dose per gram of tissue (% ID/g). For comparison, biodistribution studies were also performed for [ $^{11}\text{C}$ ]HED and [ $^{11}\text{C}$ ]EPI. These data provide some indications of the suitability of a compound as an imaging agent for human studies. For example, for cardiac imaging studies, low uptake in the liver and lungs are desirable since they are in close proximity to the heart. Similarly, high heart-to-blood ratios are desirable as they provide high-quality images of the heart wall, which aid in the interpretation of abnormalities in tracer retention. For the compounds studied, in vivo uptake into the left ventricle (LV) tended to be linearly correlated with the neuronal uptake rate in the isolated rat heart,  $K_{up}$ . A correlation coefficient  $r^2 = 0.57$  ( $P < 0.03$ ) was found between in vivo tissue concentrations in the LV at 30 min and  $K_{up}$  values measured in the isolated rat heart (Figure 7, left panel). Normalizing LV concentrations to corresponding blood concentrations for each compound, calculated LV/blood ratios at 30 min were also found to be linearly correlated with  $K_{up}$  ( $r^2 = 0.74$ ,  $P < 0.006$ ; Figure 7, right panel). These results show that, in the rat heart, measured neuronal uptake rates in the isolated rat heart are predictive of in vivo LV uptake and LV/blood ratios.

Note that extraneuronal uptake (uptake-2) was not inhibited in these biodistribution studies, so an undetermined fraction of the measured LV uptake at 30 min is due to extraneuronal uptake into myocytes. [ $^{11}\text{C}$ ]HED is a very poor substrate of uptake-2,<sup>31</sup> and more than 92% of its LV uptake at 30 min is intraneuronal.<sup>14</sup> In microPET imaging studies of compound [ $^{11}\text{C}$ ]1c in rats ( $n = 2$ ), after myocardial uptake levels peaked at around  $T = 5$  min, 21–25% of compound cleared from the heart down to a plateau of activity at the end of the 60 min study. Given the efficient intraneuronal trapping of [ $^{11}\text{C}$ ]1c in the isolated rat heart (Table 1), and previous demonstrations of

fast clearance of [ $^{123}\text{I}$ ]MIBG<sup>9</sup> and [ $^{76}\text{Br}$ ]MBBG<sup>37</sup> from the extraneuronal compartment of the rat heart, this relatively fast clearance component is likely associated with extraneuronal uptake. At  $T = 30$  min, we estimate that 92–95% of [ $^{11}\text{C}$ ]1c in the heart was intraneuronal. For compounds with lower neuronal uptake rates ( $K_{up}$ ) in the isolated rat heart, the fraction of LV uptake at  $T = 30$  min shown in Table 2 that is associated with extraneuronal uptake may be higher than for [ $^{11}\text{C}$ ]1c. However, the good correlation between neuronal uptake rates measured with uptake-2 blocked in the isolated rat heart and in vivo retention in the rat heart suggests that most of the measured LV uptake for these compounds was inside neurons.

In terms of liver uptake, compounds with a hydroxyl group at the  $\beta$ -carbon position of the side chain ([ $^{11}\text{C}$ ]HED, [ $^{11}\text{C}$ ]EPI, [ $^{11}\text{C}$ ]1d, and [ $^{11}\text{C}$ ]1e) all had substantially higher liver uptake than compounds without a  $\beta$ -carbon hydroxyl group ([ $^{11}\text{C}$ ]1b, [ $^{11}\text{C}$ ]1c, [ $^{11}\text{C}$ ]1j, and [ $^{11}\text{C}$ ]1k). This suggests that compounds without a  $\beta$ -carbon hydroxyl group would be preferable for cardiac innervation and adrenergic tumor imaging studies, since high uptake of radiotracers into the liver can be problematic for both of these imaging procedures.

In a previous study of [ $^{11}\text{C}$ ]HED uptake in rats, Law et al.<sup>38</sup> demonstrated that tissue uptake of [ $^{11}\text{C}$ ]HED was proportional to injected dose for intravenous injections containing less than 8 nmol/kg of total HED mass. For all of the biodistribution studies shown in Table 2, the injected doses of the compounds were less than 1 nmol/kg. Using the [ $^{11}\text{C}$ ]HED data as a guide, we believe that the specific activities of the compounds studied were high enough that mass effects did not cause decreases in the measured tissue uptake values.

**MicroPET Imaging Studies: Cardiac Imaging in Monkeys.** The hearts of monkeys<sup>39</sup> and humans<sup>40,41</sup> lack the extraneuronal uptake (uptake-2) pathway of catecholamines, making the monkey a more appropriate animal model for evaluating sympathetic nerve tracers than the dog, which has robust uptake-2 activity.<sup>42</sup> Cardiac imaging studies of two [ $^{11}\text{C}$ ]-

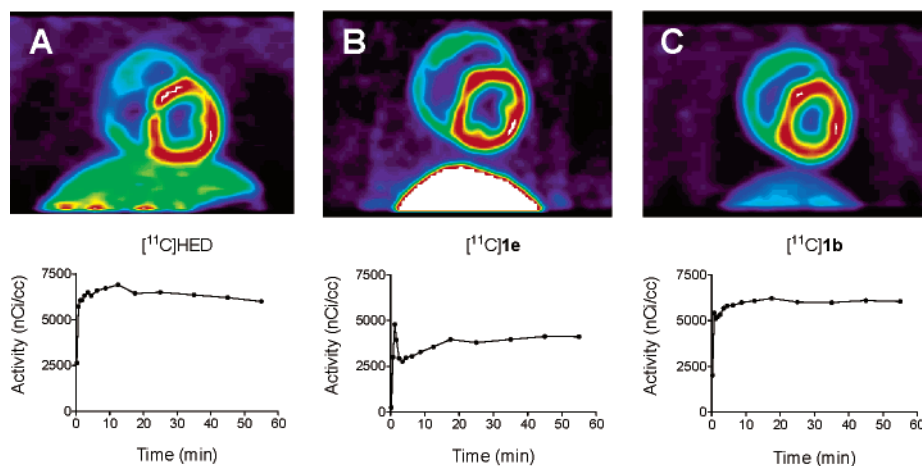


**Figure 8.** Representative PET images (coronal slice) and corresponding myocardial kinetics of selected compounds in the rhesus macaque monkey. (A)  $[^{11}\text{C}]\text{HED}$ , 5.4 mCi injected into a 5.3 kg monkey. (B)  $[^{11}\text{C}]\text{1e}$ , 4.9 mCi injected into a 4.7 kg monkey. (C)  $[^{11}\text{C}]\text{1b}$ , 4.8 mCi injected into a 5.8 kg monkey. The images are summed images of the data in the final 5 frames of the 15-frame dynamic sequence (15–60 min).

phenethylguanidines,  $[^{11}\text{C}]\text{1b}$  and  $[^{11}\text{C}]\text{1e}$ , were performed in rhesus macaque monkeys to assess their *in vivo* kinetics and imaging properties. These two compounds had the fastest and the slowest neuronal uptake rates in the isolated rat heart, respectively. For comparison,  $[^{11}\text{C}]\text{HED}$  was also studied. The imaging properties and myocardial kinetics of  $[^{11}\text{C}]\text{HED}$  ( $n = 3$ ; Figure 8A) were very similar to what is observed in cardiac PET studies in normal human subjects,<sup>43</sup> suggesting that the rhesus macaque monkey is an excellent animal model for preclinical testing of cardiac sympathetic nerve tracers. Uptake of  $[^{11}\text{C}]\text{HED}$  into cardiac sympathetic nerves was very rapid, with myocardial tissue concentrations of  $[^{11}\text{C}]\text{HED}$  staying nearly constant for the remainder of the 60 min imaging study. Heart-to-blood ratios averaged  $4.5 \pm 0.2$  at the end of the study, providing high-quality images with good contrast between the LV wall and blood in the LV chamber. Final heart-to-liver ratios were  $1.9 \pm 0.1$ . The myocardial kinetics of  $[^{11}\text{C}]\text{1e}$  were substantially different from those of  $[^{11}\text{C}]\text{HED}$  ( $n = 3$ ; Figure 8B). Heart activity peaked shortly after intravenous injection of the tracer, followed by a rapid decline of activity, evidence that some of the tracer extracted from the plasma into the tissue compartments cleared back out into the bloodstream. After this, a steady accumulation of the compound into cardiac sympathetic nerves occurred, leading to myocardial tissue concentrations at the end of the study that were  $\sim 73\%$  of the final concentrations seen with  $[^{11}\text{C}]\text{HED}$ . The relatively high final tissue concentrations of  $[^{11}\text{C}]\text{1e}$  that were achieved are remarkable considering that this compound has a neuronal uptake rate in the isolated rat heart ( $K_{\text{up}}$ ) that is only one-ninth the rate of  $[^{11}\text{C}]\text{HED}$ . This indicates that, unlike the situation in the rat heart *in vivo*, neuronal uptake rates measured for these compounds in the isolated perfused rat heart are not necessarily good predictors of final LV concentrations in the hearts of nonhuman primates. Furthermore, the shape of the time–activity curve for  $[^{11}\text{C}]\text{1e}$  in monkey heart is very encouraging in terms of applying tracer kinetic modeling methods. Clearance of some of the tracer that is initially extracted into the tissue back out into the bloodstream is a hallmark of a tracer that is not rate-limited by delivery from plasma to tissue but instead is rate-limited by neuronal uptake by NET transport. Also, the steady accumulation of the compound during the study is consistent with trapping inside storage vesicles within neurons. Thus the myocardial kinetics of  $[^{11}\text{C}]\text{1e}$  appear to be much better suited for quantifying regional nerve density in the heart by use of tracer kinetic modeling techniques than those of  $[^{11}\text{C}]\text{HED}$ . Further studies

with this promising compound, including tracer kinetic modeling of its myocardial kinetics in the monkey, are ongoing. The one drawback with  $[^{11}\text{C}]\text{1e}$  is the relatively high liver uptake that was seen; final heart-to-liver ratios were  $0.6 \pm 0.1$ . This high liver uptake is consistent with what was observed *in vivo* in the rat biodistribution studies, and appears to be due to the  $\beta$ -hydroxyl group. Finally, the myocardial kinetics of  $[^{11}\text{C}]\text{1b}$  were very similar to those of  $[^{11}\text{C}]\text{HED}$  ( $n = 1$ ; Figure 8C). Again, there was very rapid neuronal uptake of the compound early in the study, with nearly constant retention for the duration of the PET scan, with a final heart-to-blood ratio of  $\sim 4.7$ . However, of the three compounds studied,  $[^{11}\text{C}]\text{1b}$  had the lowest liver uptake, resulting in a heart-to-liver ratio of  $\sim 4.4$  and providing the highest quality images. This is the only compound of the three lacking a hydroxyl group on the  $\beta$ -carbon position, again supporting the view that it is this structural feature that causes high liver uptake. Despite the higher quality of the images with  $[^{11}\text{C}]\text{1b}$  as compared with  $[^{11}\text{C}]\text{HED}$ , since both of these compounds appear to have their neuronal uptake rate-limited by delivery from plasma to tissue, from a kinetic modeling viewpoint this tracer would not offer any advantages over  $[^{11}\text{C}]\text{HED}$ . These initial imaging studies suggest that a phenethylguanidine structure possessing *in vivo* kinetics similar to  $[^{11}\text{C}]\text{1e}$  but lacking a  $\beta$ -carbon hydroxyl group to reduce liver uptake would have optimal kinetics and imaging properties for quantitative PET studies of cardiac sympathetic innervation.

#### MicroPET Imaging Studies: Tumor Imaging in Mice.

While a slower NET transport rate is better for quantitative PET studies of cardiac innervation, rapid NET transport is a desirable tracer kinetic property for imaging studies of adrenergic tumors. In addition, long retention times inside tumors can lead to high tumor-to-background ratios, improving imaging conditions for tumor localization. Two of the compounds tested in the isolated rat heart had both a rapid NET transport rate and very long retention inside cardiac neurons,  $[^{11}\text{C}]\text{1b}$  and  $[^{11}\text{C}]\text{1c}$ . Since the rat biodistribution data suggested that LV uptake and blood levels of  $[^{11}\text{C}]\text{1c}$  were higher than those of  $[^{11}\text{C}]\text{1b}$ , but with comparable liver uptake, we chose to test the ability of  $[^{11}\text{C}]\text{1c}$  to localize adrenergic tumors in a mouse model.  $[^{11}\text{C}]\text{1c}$  was avidly taken up by pheochromocytoma (PC12) xenografts implanted in the left flank of Balb/c *nu/nu* nude mice (Figure 9). Tumor uptake of  $[^{11}\text{C}]\text{1c}$  reached peak levels of  $\sim 29\%$  ID/g of tissue within 10 min and stayed constant out to 60 min. By comparison, heart uptake at 60 min was  $\sim 17\%$  ID/g of tissue. In addition, uptake into background tissues such as the liver,



**Figure 9.** PET image of [ $^{11}\text{C}$ ]1c in a BALB/c *nu/nu* mouse with a rat pheochromocytoma (PC12) xenograft tumor in the left flank. A dose of 0.34 mCi was injected into the 25 g mouse. The image is a summed image of the data in the final 6 frames of the 12-frame dynamic sequence (15–60 min).

lungs, and gut were very low. Low background radioactivity in these structures is advantageous since it increases tumor-to-background ratios in these areas. When tumor localization studies are performed with radiolabeled MIBG, a delay of at least 24 h is imposed to improve tumor-to-background ratios, and in some cases residual uptake in the liver makes tumor localization challenging.<sup>44</sup> Thus a tracer that rapidly localizes in adrenergic tumors in less than 1 h, with very low uptake in the liver, gut, and other tissues, would represent a significant improvement over MIBG. These encouraging initial findings suggest that [ $^{11}\text{C}$ ]1c or another radiolabeled phenethylguanidine with rapid NET transport and long retention in tumors would be very useful for localizing adrenergic tumors.

## Conclusion

In summary, we synthesized and evaluated a series of [ $^{11}\text{C}$ ]-phenethylguanidines as potential PET and SPECT imaging agents for quantitative studies of cardiac sympathetic innervation or as diagnostic imaging agents for adrenergic tumors. Studies in the isolated working rat heart demonstrated that [ $^{11}\text{C}$ ]-phenethylguanidine structures with at least one hydroxyl group substitution in the phenyl ring or the  $\beta$ -carbon position of the side chain had extremely long intraneuronal retention times due to avoid accumulation and retention inside storage vesicles. In PET imaging studies in nonhuman primates, compound [ $^{11}\text{C}$ ]1e had greatly improved myocardial kinetics for quantitative tracer kinetic analyses over the currently used PET tracer [ $^{11}\text{C}$ ]-HED. PET imaging studies in mice implanted with pheochromocytoma tumors showed that compound [ $^{11}\text{C}$ ]1c was avidly taken up by the tumors, while tracer uptake into background tissues such as liver, lung, and gut were very low. We believe these encouraging initial findings with radiolabeled phenethylguanidines demonstrate that further development of these novel imaging agents is warranted, including the evaluation of new structures and a more thorough characterization of the in vivo kinetics of the most promising compounds.

## Experimental Section

$^1\text{H}$  NMR spectra were recorded on a Varian Inova instrument operating at 400 or 300 MHz. Chemical shifts ( $\delta$ ) are given in parts per million (ppm) relative to internal standard tetramethylsilane (TMS), and coupling constants ( $J$ ) are in hertz. High-resolution mass spectra were obtained on a VG-250S spectrometer by use of electrospray ionization (ESI) in positive ion mode, direct chemical ionization (DCI), or electron impact (EI) at 70 eV. Melting points were determined on a Thomas–Hoover capillary melting-point apparatus in open capillary tubes and are uncorrected. Flash chromatography utilized Merck 230–400 mesh silica gel. Thin-layer chromatography (TLC) used Analtech 0.25 mm glass-backed plates with fluorescent background. Visualization was achieved by phosphomolybdic acid (PMA) or UV illumination. High-perfor-

mance liquid chromatography (HPLC) was performed on a Hitachi pump L-7100 instrument equipped with Hitachi D-7500 integrator and Hitachi L-4000 UV detector. Radioactivity detection was done with Bioscan coincidence (model B-FC-4000) detector.

Reagents and solvents were purchased from commercial sources and used without further purification unless otherwise noted. Samples of 3-iodophenethylguanidine sulfate (MIPG) and 4-iodophenethylguanidine sulfate (PIPG) previously prepared in our laboratory were used as HPLC standards.<sup>3</sup>

**General Procedure for Rathke Reaction.** A two-necked flask was equipped with an  $\text{N}_2$  inlet tube and a reflux condenser. The end of the condenser was fitted with an  $\text{N}_2$  exit tube connected successively to an empty backup trap, a second trap containing 25% aqueous NaOH, and a third trap containing 5% aqueous NaOCl. A mixture of phenethylamine precursor (10.0 mmol) and 2-methyl-2-thiopseudourea sulfate (5.0 mmol) in water/ethanol (24 mL, 1:1 v/v) was heated under reflux with a slow stream of  $\text{N}_2$  passing through the liquid to entrain  $\text{CH}_3\text{SH}$ , until the reaction was complete. The solvent was evaporated under reduced pressure to give the solid or viscous oil product. The crude product was washed with ether (2  $\times$  30 mL), recrystallized two or three times with an appropriate solvent, and dried in vacuo to afford the pure phenethylguanidine analogue.

**Phenethylguanidine Sulfate (1a).** Yield 93% after recrystallization from water: mp 168–171  $^\circ\text{C}$  (lit.<sup>45</sup> 168–173  $^\circ\text{C}$ );  $^1\text{H}$  NMR (400 MHz,  $\text{CD}_3\text{OD}$ )  $\delta$  2.88 (t,  $J$  = 7.5 Hz, 2H), 3.39 (t,  $J$  = 7.5 Hz, 2H), 7.19–7.31 (m, 5H); HRMS calcd for  $\text{C}_9\text{H}_{13}\text{N}_3$  163.1109 ( $\text{M}^+$ ), obsd 163.1103.

**4-Hydroxyphenethylguanidine Sulfate (1c).** Yield 85% after recrystallization from ethanol: mp 243–247  $^\circ\text{C}$  (lit.<sup>46</sup> 245–250  $^\circ\text{C}$ );  $^1\text{H}$  NMR (400 MHz,  $\text{CD}_3\text{OD}$ )  $\delta$  2.77 (t,  $J$  = 7.3 Hz, 2H), 3.34 (t,  $J$  = 7.3 Hz, 2H), 6.72 (d,  $J$  = 8.6 Hz, 2H), 7.07 (d,  $J$  = 8.6 Hz, 2H); HRMS calcd for  $\text{C}_9\text{H}_{13}\text{N}_3\text{O}$  180.1137 ( $\text{M} + \text{H}^+$ ), obsd 180.1131.

**(-)- $\beta$ -Hydroxyphenethylguanidine Sulfate (1d).** Yield 52% after recrystallization from ethanol/water: mp 229–231  $^\circ\text{C}$  (lit.<sup>23</sup> 228  $^\circ\text{C}$ );  $[\alpha]_{\text{D}}^{23}$   $-36^\circ$  in 50% aqueous MeOH;  $^1\text{H}$  NMR (300 MHz,  $\text{CD}_3\text{OD}$  + 3 drops of  $\text{DMSO}-d_6$ )  $\delta$  3.28 (dd,  $J$  = 13.8, 8.2 Hz, 1H), 3.38 (dd,  $J$  = 13.8, 3.5 Hz, 1H), 4.81 (dd,  $J$  = 8.2, 3.5 Hz, 1H), 7.25–7.45 (m, 5H); HRMS calcd for  $\text{C}_9\text{H}_{13}\text{N}_3\text{O}$  180.1137 ( $\text{M} + \text{H}^+$ ), obsd 180.1131.

**(-)- $\beta$ -Guanyl-*m*-octopamine (1e).** Yield 32% after recrystallization from ethanol/water: mp 225–227  $^\circ\text{C}$ ;  $[\alpha]_{\text{D}}^{23}$   $-28^\circ$  in 50% aqueous MeOH;  $^1\text{H}$  NMR (300 MHz,  $\text{CD}_3\text{OD}$  + 3 drops of  $\text{DMSO}-d_6$ )  $\delta$  3.30 (dd,  $J$  = 13.9, 8.0 Hz, 1H), 3.38 (dd,  $J$  = 13.9, 3.7 Hz, 1H), 4.81 (dd,  $J$  = 8.0, 3.7 Hz, 1H), 6.69 (ddd,  $J$  = 7.8, 2.4, 1.0 Hz, 1H), 6.70–6.89 (m, 2H), 7.16 (t,  $J$  = 7.8 Hz, 1H); HRMS calcd for  $\text{C}_9\text{H}_{13}\text{N}_3\text{O}_2$  196.1086 ( $\text{M} + \text{H}^+$ ), obsd 196.1089.

**4-Methoxyphenethylguanidine Sulfate (1f).** Yield 74% after recrystallization from water: mp 181–182  $^\circ\text{C}$  (lit.<sup>46</sup> 183–184  $^\circ\text{C}$ , lit.<sup>47</sup> 210–211  $^\circ\text{C}$ );  $^1\text{H}$  NMR (400 MHz,  $\text{CD}_3\text{OD}$ )  $\delta$  2.81 (t,  $J$  = 7.3 Hz, 2H), 3.36 (t,  $J$  = 7.3 Hz, 2H), 3.75 (s, 3H), 6.84 (d,  $J$  = 8.8 Hz, 2H), 7.17 (d,  $J$  = 8.8 Hz, 2H); HRMS calcd for  $\text{C}_{10}\text{H}_{15}\text{N}_3\text{O}$  194.1293 ( $\text{M} + \text{H}^+$ ), obsd 194.1287.

**3-Fluorophenethylguanidine Sulfate (1g).** Yield 78% after recrystallization from ethanol/water: mp 188–189  $^\circ\text{C}$ ;  $^1\text{H}$  NMR (400 MHz,  $\text{CD}_3\text{OD}$ )  $\delta$  2.90 (t,  $J$  = 7.3 Hz, 2H), 3.41 (t,  $J$  = 7.3 Hz, 2H), 6.94 (td,  $J$  = 8.4, 2.1 Hz, 1H), 7.04 (dd,  $J$  = 10.0, 2.1 Hz, 1H), 7.09 (d,  $J$  = 7.8 Hz, 1H), 7.30 (td,  $J$  = 7.8, 2.1 Hz, 1H); HRMS calcd for  $\text{C}_9\text{H}_{12}\text{FN}_3$  181.1015 ( $\text{M}^+$ ), obsd 181.1010.

**4-Fluorophenethylguanidine Sulfate (1h).** Yield 86% after recrystallization from water: mp 217–221  $^\circ\text{C}$ ;  $^1\text{H}$  NMR (400 MHz,  $\text{CD}_3\text{OD}$ )  $\delta$  2.87 (t,  $J$  = 7.3 Hz, 2H), 3.38 (t,  $J$  = 7.3 Hz, 2H), 7.02 (d,  $J$  = 8.8 Hz, 2H), 7.28 (dd,  $J$  = 8.8, 5.4 Hz, 2H); HRMS calcd for  $\text{C}_9\text{H}_{12}\text{FN}_3$  182.1094 ( $\text{M} + \text{H}^+$ ), obsd 182.1091.

**2-Fluorophenethylguanidine Sulfate (1i).** Yield 80% after recrystallization from water: mp 185–186  $^\circ\text{C}$ ;  $^1\text{H}$  NMR (400 MHz,  $\text{CD}_3\text{OD}$ )  $\delta$  2.94 (t,  $J$  = 7.2 Hz, 2H), 3.42 (t,  $J$  = 7.2 Hz, 2H), 7.06 (td,  $J$  = 8.4, 2.1 Hz, 1H), 7.05 (td,  $J$  = 8.6, 1.2 Hz, 1H), 7.12 (td,  $J$  = 7.4, 1.2 Hz, 1H), 7.25 (m, 1H), 7.33 (td,  $J$  = 7.6, 1.6 Hz, 1H); HRMS calcd for  $\text{C}_9\text{H}_{12}\text{FN}_3$  181.1015 ( $\text{M}^+$ ), obsd 181.1011.



**General Procedure for Preparation of *N,N'*-Bis(benzyloxycarbonyl)-*N''*-phenethylguanidines (3b, 3j, 3k).** To a solution of phenethylamine hydrochloride analogue (3.54 mmol) and triethylamine (14.2 mmol) in dried *N,N*-dimethylformamide (DMF) (20 mL) was added in portion 1,3-bis(benzyloxycarbonyl)-2-methyl-2-thiopseudourea (3.71 mmol) at room temperature. The reaction mixture was stirred overnight and then diluted with ethyl acetate (60 mL). The resulting solution was washed with saturated NaHCO<sub>3</sub> solution (80 mL) and extracted with ethyl acetate (2 × 100 mL). The combined extracts were dried over anhydrous Na<sub>2</sub>SO<sub>4</sub> and concentrated under reduced pressure. The residue was flash-chromatographed on silica gel, eluted with a mixture of ethyl acetate and hexane to afford *N,N'*-bis(benzyloxycarbonyl)-*N''*-3-hydroxyphenethylguanidine.

***N,N'*-Bis(benzyloxycarbonyl)-*N''*-3-hydroxyphenethylguanidine (3b).** Yield 99% after flash chromatography with a 20–30% ethyl acetate/hexane gradient: mp 130–132 °C; <sup>1</sup>H NMR (300 MHz, DMSO-*d*<sub>6</sub>) δ 2.73 (t, *J* = 7.0 Hz, 2H), 3.53 (q, *J* = 7.0 Hz, 2H), 5.05 (s, 2H), 5.20 (s, 2H), 6.59–6.64 (m, 3H), 7.07 (t, *J* = 7.7 Hz, 1H), 7.30–7.43 (m, 10H), 8.44 (t, *J* = 5.6 Hz, 1H), 9.30 (s, 1H), 11.60 (s, 1H); HRMS calcd for C<sub>25</sub>H<sub>25</sub>N<sub>3</sub>O<sub>5</sub> 470.1692 (M + Na)<sup>+</sup>, obsd 470.1691.

***N,N'*-Bis(benzyloxycarbonyl)-*N''*-4-fluoro-3-hydroxyphenethylguanidine (3j).** Yield 97% after flash chromatography with a 20–30% ethyl acetate/hexane gradient: mp 112–115 °C; <sup>1</sup>H NMR (300 MHz, DMSO-*d*<sub>6</sub>) δ 2.72 (t, *J* = 7.0 Hz, 2H), 3.51 (q, *J* = 6.7 Hz, 2H), 5.05 (s, 2H), 5.20 (s, 2H), 6.59–6.63 (m, 1H), 6.80 (dd, *J* = 8.5, 1.3 Hz, 1H), 7.02 (dd, *J* = 11.4, 8.5 Hz, 1H), 7.30–7.41 (m, 10H), 8.44 (t, *J* = 5.6 Hz, 1H), 9.75 (s, 1H), 11.61 (s, 1H); HRMS calcd for C<sub>25</sub>H<sub>24</sub>FN<sub>3</sub>O<sub>5</sub> 488.1598 (M + Na)<sup>+</sup>, obsd 488.1604.

***N,N'*-Bis(benzyloxycarbonyl)-*N''*-6-fluoro-3-hydroxyphenethylguanidine (3k).** Yield 100% after flash chromatography with a 20–30% ethyl acetate/hexane gradient: mp 133–135 °C; <sup>1</sup>H NMR (300 MHz, DMSO-*d*<sub>6</sub>) δ 2.78 (t, *J* = 7.0 Hz, 2H), 3.54 (q, *J* = 6.6 Hz, 2H), 5.05 (s, 2H), 5.20 (s, 2H), 6.58–6.66 (m, 2H), 6.93 (t, *J* = 9.2 Hz, 1H), 7.29–7.42 (m, 10H), 8.48 (t, *J* = 5.5 Hz, 1H), 9.32 (s, 1H), 11.61 (s, 1H); HRMS calcd for C<sub>25</sub>H<sub>24</sub>FN<sub>3</sub>O<sub>5</sub> 488.1598 (M + Na)<sup>+</sup>, obsd 488.1594.

***N,N'*-Bis(benzyloxycarbonyl)-*N''*-4-hydroxybenzylguanidine.** Yield 100% after flash chromatography with a 30% ethyl acetate/hexane gradient: mp 82–83 °C; <sup>1</sup>H NMR (300 MHz, DMSO-*d*<sub>6</sub>) δ 4.42 (t, *J* = 5.6 Hz, 2H), 5.04 (s, 2H), 5.20 (s, 2H), 6.71 (d, *J* = 8.5 Hz, 2H), 7.13 (d, *J* = 8.5 Hz, 2H), 7.30–7.43 (m, 10H), 8.48 (t, *J* = 5.6 Hz, 1H), 9.36 (s, 1H), 11.59 (s, 1H); HRMS calcd for C<sub>24</sub>H<sub>23</sub>N<sub>3</sub>O<sub>5</sub> 456.1535 (M + Na)<sup>+</sup>, obsd 456.1524.

**General Procedure for Preparation of Phenethylguanidines (1b, 1j, 1k) via Hydrogenolysis.** *N,N'*-Bis(benzyloxycarbonyl)-*N''*-3-hydroxyphenethylguanidine (1.54 g, 3.44 mmol) was dissolved in ethyl acetate (10 mL) and methanol (30 mL), and 10% palladium on activated carbon (300 mg) was added. The mixture was hydrogenated at 40 psi for 5 h. After filtration through the Celite pad, the solution was concentrated under reduced pressure to afford 3-hydroxyphenethylguanidine (559 mg, 3.12 mmol, 91% yield) as a viscous oil, which was used for the next step without further purification. To a solution of 3-hydroxyphenethylguanidine (412 mg, 2.30 mmol) in ethanol (10 mL) was added dropwise a solution of 0.505 N H<sub>2</sub>SO<sub>4</sub> in H<sub>2</sub>O (2.28 mL, 1.15 mmol). After the mixture was stirred for 5 min, a solution was concentrated under reduced pressure. The crude solid product was recrystallized from ethanol to afford 409 mg (78%) of 3-hydroxyphenethylguanidine sulfate **1b** as a white solid.

**3-Hydroxyphenethylguanidine Sulfate<sup>48</sup> (1b).** Yield 78% after recrystallization from ethanol: mp 185–187 °C; <sup>1</sup>H NMR (400 MHz, CD<sub>3</sub>OD + 3 drops of DMSO-*d*<sub>6</sub>) δ 2.80 (t, *J* = 7.2 Hz, 2H), 3.38 (t, *J* = 7.2 Hz, 2H), 6.64 (td, *J* = 7.8, 1.5 Hz, 1H), 6.72 (d, *J* = 7.8 Hz, 1H), 6.73 (s, 1H), 7.11 (t, *J* = 7.8 Hz, 1H); HRMS calcd for C<sub>9</sub>H<sub>13</sub>N<sub>3</sub>O 180.1137 (M + H)<sup>+</sup>, obsd 180.1136.

**4-Fluoro-3-hydroxyphenethylguanidine Sulfate (1j).** Yield 63% after recrystallization from ethanol: mp 178–183 °C; <sup>1</sup>H NMR (400 MHz, CD<sub>3</sub>OD + 3 drops of DMSO-*d*<sub>6</sub>) δ 2.84 (t, *J* = 7.0 Hz,

2H), 3.40 (t, *J* = 7.0 Hz, 2H), 6.67 (m, 1H), 6.87 (dd, *J* = 8.5, 2.0 Hz, 1H), 6.95 (dd, *J* = 11.1, 8.5 Hz, 1H); HRMS calcd for C<sub>9</sub>H<sub>12</sub>FN<sub>3</sub>O 198.1043 (M + H)<sup>+</sup>, obsd 198.1037.

**6-Fluoro-3-hydroxyphenethylguanidine Sulfate (1k).** Yield 82% after recrystallization from ethanol: mp 215–216 °C; <sup>1</sup>H NMR (400 MHz, CD<sub>3</sub>OD + 3 drops of DMSO-*d*<sub>6</sub>) δ 2.84 (t, *J* = 7.0 Hz, 2H), 3.40 (t, *J* = 7.0 Hz, 2H), 6.62 (td, *J* = 9.0, 3.5 Hz, 1H), 6.78 (dd, *J* = 6.2, 3.5 Hz, 1H), 6.88 (t, *J* = 9.0 Hz, 1H); HRMS calcd for C<sub>9</sub>H<sub>12</sub>FN<sub>3</sub>O 190.1043 (M + H)<sup>+</sup>, obsd 198.1038.

**4-Hydroxybenzylguanidine Sulfate (5).** Yield 69% after recrystallization from ethanol: mp 255–257 °C (lit.<sup>49</sup> 260–262 °C); <sup>1</sup>H NMR (400 MHz, CD<sub>3</sub>OD + 3 drops of DMSO-*d*<sub>6</sub>) δ 2.84 (t, *J* = 7.0 Hz, 2H), 3.40 (t, *J* = 7.0 Hz, 2H), 6.62 (td, *J* = 9.0, 3.5 Hz, 1H), 6.78 (dd, *J* = 6.2, 3.5 Hz, 1H), 6.88 (t, *J* = 9.0 Hz, 1H); HRMS calcd for C<sub>9</sub>H<sub>12</sub>FN<sub>3</sub>O 190.1043 (M + H)<sup>+</sup>, obsd 198.1038.

**Radiosynthesis of <sup>11</sup>C-Labeled Phenethylguanidines ([<sup>11</sup>C]1a–m).** The radiosynthesis of <sup>11</sup>C-labeled phenethylguanidines ([<sup>11</sup>C]1a–m) was achieved with [<sup>11</sup>C]cyanogen bromide as the labeling reagent, on the basis of previously described methods with some modifications.<sup>29</sup> No-carrier-added [<sup>11</sup>C]CO<sub>2</sub> was prepared by proton bombardment of a nitrogen gas target [<sup>14</sup>N(p,α)<sup>11</sup>C], and catalytically reduced with hydrogen over a nickel catalyst at 385 °C to form [<sup>11</sup>C]CH<sub>4</sub>. [<sup>11</sup>C]CH<sub>4</sub> was mixed with ammonia and passed over a platinum catalyst held at 950 °C to convert [<sup>11</sup>C]CH<sub>4</sub> into [<sup>11</sup>C]-HCN, which was then passed through a quartz glass tube containing 0.4 g of PyBr<sub>3</sub> to form [<sup>11</sup>C]CNBr. While the conversion rate of [<sup>11</sup>C]CO<sub>2</sub> to [<sup>11</sup>C]CH<sub>4</sub> was >99%, conversion rates of [<sup>11</sup>C]CH<sub>4</sub> to [<sup>11</sup>C]HCN were variable, ranging from 47% to 85%. Starting quantities of [<sup>11</sup>C]CNBr were estimated to range from 550 to 1000 mCi. In a 1.0 mL reaction vial, 1.0–1.5 mg of phenethylamine precursor as the free base or hydrochloride salt was dissolved in 0.25 mL of borate buffer (pH 8.0). [<sup>11</sup>C]CNBr was collected in the reaction vial at room temperature in N<sub>2</sub> carrier (30 mL/min) until radioactivity in the vial had peaked (~3.5 min). The resulting mixture was heated at 80–85 °C for 5 min and then cooled to about 40 °C. After 0.25 mL of 35% NH<sub>4</sub>Br in 25% NH<sub>4</sub>OH was added to the reaction vial, the vial was sealed and heated at 130–135 °C for 5 min to yield the desired [<sup>11</sup>C]phenethylguanidine. The mixture was cooled to ambient temperature and then injected onto a Phenomenex Synergi 4 μm Hydro RP column, 50 × 4.6 mm or 150 × 4.6 mm, eluted with 0.1 M ammonium acetate buffer or 60 mM sodium phosphate buffer with 0–10% ethanol. Column effluent was monitored for radioactivity and UV absorbance (224 or 241 nm). Retention times (*R*<sub>t</sub>) ranged from 4.0 to 9.5 min at flow rates of 1.0 to 3.0 mL/min, depending upon the differing polarities of the radiotracers. Corrected radiochemical yields were 2.5–6% (relative to [<sup>11</sup>C]CO<sub>2</sub> produced), with specific activities of >500 Ci/mmol at end of synthesis (EOS). Radiochemical and chemical purities were >98%. For most compounds, 25–60 mCi of activity was obtained at EOS, with synthesis times of 35–40 min.

**Radiosynthesis of [<sup>11</sup>C]HED and [<sup>11</sup>C]EPI.** [<sup>11</sup>C]HED was synthesized by *N*-methylation of (–)-metaraminol as the free base, by use of previously described methods<sup>14</sup> with a few modifications. Briefly, [<sup>11</sup>C]methyl triflate<sup>50</sup> in a N<sub>2</sub> carrier gas stream was bubbled at room temperature through 0.25 mL of dimethylformamide (DMF) containing 1.0 mg of (–)-metaraminol until the radioactivity trapped in the reaction vial reached a maximum (~4 min). Because of the high reactivity of [<sup>11</sup>C]methyl triflate, the reaction to form HED is extremely rapid and no heating of the reaction vial is necessary. HED was purified by HPLC (Phenomenex Partisil 10 μm SCX 4.6 × 250 mm column; mobile phase 60 mM NaH<sub>2</sub>PO<sub>4</sub> monohydrate; flow rate 2.0 mL/min; *R*<sub>t</sub> ~ 6 min). Total synthesis time, including HPLC purification and product formulation, was ~35 min. Corrected radiochemical yields were 20–25%, with radiochemical purity >98% and specific activity >500 Ci/mmol. [<sup>11</sup>C]-EPI was synthesized under comparable conditions, except the [<sup>11</sup>C]methyl triflate was passed through 0.25 mL of dimethyl sulfoxide (DMSO) containing 1.0 mg of (–)-norepinephrine as the free base. HPLC purification conditions were the same as used for [<sup>11</sup>C]HED except the mobile phase was 25 mM NaH<sub>2</sub>PO<sub>4</sub> monohydrate; flow rate 3.0 mL/min; *R*<sub>t</sub> ~ 6 min. Corrected radiochemical

yields, radiochemical purities, and specific activities were comparable to those achieved with [<sup>11</sup>C]HED.

**Animal Care.** The care of all animals used in this study was done in accordance with the Animal Welfare Act and the National Institutes of Health's *Guide for the Care and Use of Laboratory Animals*.<sup>51</sup> Animal protocols were approved by the University Committee on Use and Care of Animals (UCUCA) at the University of Michigan.

**Isolated Rat Heart Studies.** Hearts from male Sprague-Dawley rats (225–500 g) were perfused under moderate workload conditions (7.3 mmHg preload, 73 mmHg afterload) by use of a working heart preparation based on the system of Taegtmeier et al.<sup>52</sup> Two separate perfusion circuits were used in parallel, connected to the left atrial cannula with a 3-way connector to allow for rapid switching from one perfusion circuit to the other. The perfusion medium was Krebs–Henseleit (KH) bicarbonate buffer (118 nM NaCl, 4.7 mM KCl, 2.55 mM CaCl<sub>2</sub>, 1.2 mM MgSO<sub>4</sub>, 1.2 mM K<sub>2</sub>H<sub>2</sub>PO<sub>4</sub>, and 25 mM NaHCO<sub>3</sub>) containing 5 mM glucose and oxygenated with a 95% O<sub>2</sub>/5% CO<sub>2</sub> gas mixture. Corticosterone (54 μM) was added to the perfusate to block extraneuronal uptake (uptake-2) of the radiotracers into the rat myocardium.<sup>30</sup>

Radioactivity in the heart was measured externally by use of a pair of cesium fluoride (CsF) scintillation detectors (Crismatec 51Y51; Saint-Gobain, Nemours, France), with the front faces of the two CsF detectors directly opposing each other and the heart centered between them. Each detector was enclosed in a large cylindrical lead collimator (2 cm wall thickness, 25 cm long) to minimize detected counts originating from radioactive sources outside the heart. Two coincidence detection circuits were established between the detectors by use of standard Nuclear Instrumentation Module (NIM) electronic modules. One circuit measured total coincident events between the two detectors (true + random coincident events), and the second measured only random coincident events. A computer-driven data acquisition system interfaced to the NIM-module coincidence circuits was used to acquire and record the whole-heart radioactivity data throughout the study.<sup>37</sup>

Hearts were initially perfused for a 30 min stabilization period with KH buffer in the first of the two perfusion circuits. During this time, the [<sup>11</sup>C]-labeled tracer being studied was added to 1.0 L of KH buffer circulating in the second perfusion circuit and allowed to mix for several minutes. Three 1.0 mL aliquots were then drawn from the second perfusion circuit and counted in a γ counter (Perkin-Elmer MINAXI AutoGamma 5500) to determine the radioactivity concentration in the perfusate (C<sub>p</sub>). Depending on the radiotracer being studied, radioactivity concentrations of 2.0–12.0 μCi/mL perfusate were used. After data acquisition from the CsF detectors was initiated, the heart was rapidly switched to the second perfusion circuit to begin a constant infusion of the [<sup>11</sup>C]-labeled tracer. After 10 min of constant infusion, the heart was switched back to the first perfusion circuit for 120 min to study clearance of the tracer from the heart.

The acquired whole-heart radioactivity data (counts per second, cps) at each time point were converted to an apparent distribution volume (ADV; milliliters of perfusate per gram wet weight) by dividing by the perfusate radioactivity concentration C<sub>p</sub> (microcuries per milliliter of perfusate), the external detection system calibration factor Z<sub>calib</sub> (counts per second per microcurie), and the measured wet mass of the heart M<sub>w</sub> (grams wet weight). Neuronal uptake rates of the radiotracers (K<sub>up</sub>; milliliters of perfusate per minute per gram wet weight) were calculated by fitting the ADV data between t = 1 min and t = 4 min of the 10 min constant infusion phase of the experiment to a line. Clearance rates were estimated by fitting the ADV data during the clearance phase of the study to multiple exponential decay processes. The exponential clearance rate constants (λ<sub>i</sub>) were used to calculate corresponding clearance half-times (T<sub>1/2</sub> = ln 2/λ<sub>i</sub>). The slowest estimated rate, associated with clearance from sympathetic neurons, is the rate reported for each compound.

**Tissue Distribution Studies in Rat.** Sprague-Dawley rats (200–225 g) were purchased from Charles River Laboratories, Inc.,

Wilmington, MA. For each radiotracer evaluated, five rats under light ether anesthesia received bolus tail-vein injections of 50–350 μCi of tracer in 0.05–0.10 mL of isotonic 60 mM sodium phosphate buffer, pH 4.5. Rats were killed by decapitation while under anesthesia at 30 min after tracer injection. Organs and blood samples were quickly removed from the rat carcasses and placed in previously weighed tubes. Tubes were weighed again to determine tissue masses and then counted in a γ-counter (MINAXI Auto-Gamma 5500; Perkin-Elmer, Wellesley, MA). γ-Counter data were corrected for radioactive decay and normalized to tissue mass to determine radiotracer tissue concentrations, expressed as percentage injected dose per gram of tissue (% ID/g).

**Cardiac PET Imaging Studies.** Cardiac PET studies were performed in rhesus macaque monkeys by use of a microPET P4 primate scanner (Siemens/CTI Concorde Microsystems, Knoxville, TN). The monkey was anesthetized with isoflurane and intubated, and the tail was shaved and disinfected for placement of a percutaneous angiocatheter. Ophthalmic ointment was administered in the eyes and the animal was placed on a recirculating water blanket on the scanner bed to maintain body temperature. After the monkey was positioned in the scanner gantry, a 20 min transmission scan was acquired by use of a rotating <sup>68</sup>Ge source to generate attenuation correction data. Next, 5–6 mCi of radiotracer was injected via the catheter. Starting just before tracer injection, emission data from the PET scanner was collected in list mode for 60 min. The list-mode PET data were rebinned into a 15-frame dynamic sequence (4 × 30 s, 3 × 60 s, 2 × 150 s, 2 × 300 s, 4 × 600 s). Images were reconstructed by use of an OSEM/3D-MAP reconstruction algorithm. Regions of interest were drawn on the left ventricle wall (LV), left ventricle chamber (blood), and liver to generate time–activity curves for each tissue from the dynamic PET images.

**PET Imaging Studies of Adrenergic Tumors.** Rat pheochromocytoma cells (PC12) were obtained from ATCC (Manassas, VA) and cultured under conditions recommended by ATCC. Athymic BALB/c *nu/nu* mice (n = 4, Charles River, Wilmington, MA), 4–6 weeks old, were injected subcutaneously with 2.0–2.5 × 10<sup>6</sup> PC12 cells in 100 μL of phosphate-buffered saline (PBS) in their left abdominal flank. After 4–5 weeks, when PC12 xenografts were 10–20 mm diameter and body weights were 23–25 g, PET imaging studies were performed with a microPET R4 rodent scanner (Siemens/CTI Concorde Microsystems, Knoxville, TN). Anesthesia was induced with 5% isoflurane and maintained during the study with 2% isoflurane. The mice were placed on a recirculating water blanket on the scanner bed to maintain body temperature, and ophthalmic ointment was administered in the eyes. A 20 min transmission scan was acquired by use of a rotating <sup>68</sup>Ge source to generate attenuation correction data. Next, 0.3–0.4 mCi of radiotracer was injected via a tail vein catheter. The list-mode PET data were rebinned into a 12-frame dynamic sequence (5 × 120 s, 4 × 300 s, 3 × 600 s). Images were reconstructed by use of an OSEM/3D-MAP reconstruction algorithm.

**Acknowledgment.** We thank the staff of the University of Michigan Cyclotron/PET Facility for their support in the preparation and evaluation of all radiopharmaceuticals included in this work. We also thank Donald Wieland, Robert Koeppel, Michael Kilbourn, Scott Snyder, and Doug Jewett for their helpful advice. This work was supported by Grant R01-HL079540 from the National Heart Lung and Blood Institute, National Institutes of Health, Bethesda, MD.

**Supporting Information Available:** Chemical purity measurements determined by HPLC analysis. This material is available free of charge via the Internet at <http://pubs.acs.org>.

## References

- 1) Wieland, D. M.; Wu, J.; Brown, L. E.; Mangner, T. J.; Swanson, D. P.; et al. Radiolabeled adrenergic neuron-blocking agents: adrenomodulatory imaging with [<sup>131</sup>I]iodobenzylguanidine. *J. Nucl. Med.* **1980**, *21*, 349–353.

- (2) Sisson, J. C.; Frager, M. S.; Valk, T. W.; Gross, M. D.; Swanson, D. P.; et al. Scintigraphic localization of pheochromocytoma. *N. Engl. J. Med.* **1981**, *305*, 12–17.
- (3) Wieland, D. M.; Mangner, T. J.; Inbasekaran, M. N.; Brown, L. E.; Wu, J. Adrenal medulla imaging agents: a structure-distribution relationship study of radiolabeled aralkylguanidines. *J. Med. Chem.* **1984**, *27*, 149–155.
- (4) Tobes, M. C.; Jaques, S.; Wieland, D. M.; Sisson, J. C. Effect of uptake-one inhibitors on the uptake of norepinephrine and metaiodobenzylguanidine. *J. Nucl. Med.* **1985**, *26*, 897–907.
- (5) Bönisch, H.; Harder, R. Binding of <sup>3</sup>H-desipramine to the neuronal noradrenaline carrier of rat pheochromocytoma cells (PC-12 cells). *Naunyn-Schmiedeberg's Arch. Pharmacol.* **1986**, *334*, 403–411.
- (6) Lode, H. N.; Bruchelt, G.; Sietz, G.; Gebhardt, S.; Gekeler, V.; et al. Reverse transcriptase-polymerase chain reaction (RT-PCR) analysis of monoamine transporters in neuroblastoma cell lines: correlations to meta-iodobenzylguanidine (MIBG) uptake and tyrosine hydroxylase gene expression. *Eur. J. Cancer* **1995**, *31A*, 586–590.
- (7) Wieland, D. M.; Brown, L. E.; Rogers, W. L.; Worthington, K. C.; Wu, J.-L.; et al. Myocardial imaging with a radioiodinated norepinephrine storage analog. *J. Nucl. Med.* **1981**, *22*, 22–31.
- (8) Flotats, A.; Carrió, I. Cardiac neurotransmission SPECT imaging. *J. Nucl. Cardiol.* **2004**, *11*, 587–602.
- (9) DeGrado, T. R.; Zalutsky, M. R.; Vaidyanathan, G. Uptake mechanisms of meta-[<sup>123</sup>I]iodobenzylguanidine in isolated rat heart. *Nucl. Med. Biol.* **1995**, *22*, 1–12.
- (10) Nakajo, M.; Shimabukuro, K.; Yoshimura, H.; Yonekura, R.; Nakabeppu, Y.; et al. Iodine-131 metaiodobenzylguanidine intra- and extravesicular accumulation in the rat heart. *J. Nucl. Med.* **1986**, *27*, 84–89.
- (11) Erickson, J. D.; Schäfer, M. K. H.; Bonner, T. I.; Eiden, L. E.; Weihe, E. Distinct pharmacological properties and distribution in neurons and endocrine cells of two isoforms of the human vesicular monoamine transporter. *Proc. Natl. Acad. Sci. U.S.A.* **1996**, *93*, 5166–5171.
- (12) Wieland, D. M.; Rosenspire, K. C.; Hutchins, G. D.; Van Dort, M.; Rothley, J. M.; et al. Neuronal mapping of the heart with 6-[<sup>18</sup>F]-fluorometaraminol. *J. Med. Chem.* **1990**, *33*, 956–964.
- (13) Goldstein, D. S.; Chang, P. C.; Eisenhofer, G.; Miletich, R.; Finn, R.; et al. Positron emission tomographic imaging of cardiac sympathetic innervation and function. *Circulation* **1990**, *81*, 1606–1621.
- (14) Rosenspire, K. C.; Haka, M. S.; Van Dort, M. E.; Jewett, D. M.; Gildersleeve, D. L.; et al. Synthesis and preliminary evaluation of carbon-11-meta-hydroxyephedrine: A false transmitter agent for heart neuronal imaging. *J. Nucl. Med.* **1990**, *31*, 1328–1334.
- (15) Chakraborty, P. K.; Gildersleeve, D. L.; Jewett, D. M.; Toorongian, S. A.; Kilbourn, M. R.; et al. High yield synthesis of high specific activity R-(−)-[<sup>11</sup>C]epinephrine for routine PET studies in humans. *Nucl. Med. Biol.* **1993**, *20*, 939–944.
- (16) Del Rosario, R. B.; Jung, Y.-W.; Chakraborty, P. K.; Sherman, P. S.; Wieland, D. M. Synthesis and preliminary evaluation of [C-11] phenylephrine for mapping heart neuronal function. *Nucl. Med. Biol.* **1996**, *23*, 611–616.
- (17) Loc'h, C.; Mardon, K.; Valette, H.; Brutusco, C.; Merlet, P.; et al. Preparation and pharmacological characterization of 76Br-meta-bromobenzylguanidine (76Br-MBBG). *Nucl. Med. Biol.* **1994**, *21*, 49–55.
- (18) Garg, P. K.; Garg, S.; Zalutsky, M. R. Synthesis and preliminary evaluation of para- and meta-[<sup>18</sup>F]fluorobenzylguanidine. *Nucl. Med. Biol.* **1994**, *21*, 97–103.
- (19) Raffel, D. M.; Wieland, D. M. Assessment of cardiac sympathetic nerve integrity with positron emission tomography. *Nucl. Med. Biol.* **2001**, *28*, 541–559.
- (20) Bengel, F. M.; Schwaiger, M. Assessment of cardiac sympathetic neuronal function using PET imaging. *J. Nucl. Cardiol.* **2004**, *11*, 603–616.
- (21) Raffel, D. M.; Chen, W.; Sherman, P. S.; Gildersleeve, D. L.; Jung, Y. W. Dependence of cardiac <sup>11</sup>C-meta-hydroxyephedrine retention on norepinephrine transporter density. *J. Nucl. Med.* **2006**, *47*, 1490–1496.
- (22) Fielden, R.; Green, A. L. The effects of some aralkylguanidines in mice. *Br. J. Pharmacol.* **1965**, *24*, 408–417.
- (23) Green, A. L.; Fielden, R.; Bartlett, D. C.; Cozens, M. J.; Eden, R. J.; et al. New norepinephrine-depleting agents.  $\beta$ -hydroxyphenethylguanidine and related compounds. *J. Med. Chem.* **1967**, *10*, 1006–1008.
- (24) Costa, E.; Kunstman, R.; Gessa, G. L.; Brodie, B. B. Structural requirements for bremelium and guanethidine-like activity in a series of guanidine derivatives. *Life Sci.* **1962**, *3*, 75–80.
- (25) Konkel, J. T.; Fan, J.; Jayachandran, B.; Kirk, K. L. Syntheses of 6-fluoro-meta-tyrosine and of its metabolites. *J. Fluorine Chem.* **2002**, *115*, 27–32.
- (26) Rathke, B. Ueber Verbindungen des Schwefelharstoffes. *Ber. Dtsch. Chem. Ges.* **1884**, *17*, 297–309.
- (27) Greenhill, J. V.; Lue, P. Amidines and guanidines in medicinal chemistry. *Prog. Med. Chem.* **1993**, *30*, 203–326.
- (28) Su, W. A convenient synthesis of di-(benzyloxy carbonyl)-protected guanidines. *Synth. Commun.* **1996**, *26*, 407–461.
- (29) Westerberg, G.; Långström, B. Synthesis of meta-iodobenzyl [<sup>11</sup>C]-guanidine. *J. Labeled Compds. Radiopharm.* **1997**, *39*, 525–529.
- (30) Salt, P. J. Inhibition of noradrenaline uptake<sub>2</sub> in the isolated rat heart by steroids, clonidine and methoxylated phenylethylamines. *Eur. J. Pharmacol.* **1972**, *20*, 329–340.
- (31) DeGrado, T. R.; Hutchins, G. D.; Toorongian, S. A.; Wieland, D. M.; Schwaiger, M. Myocardial kinetics of carbon-11-meta-hydroxyephedrine: retention mechanisms and effects of norepinephrine. *J. Nucl. Med.* **1993**, *34*, 1287–1293.
- (32) Nguyen, N. T. B.; DeGrado, T. R.; Chakraborty, P.; Wieland, D. M.; Schwaiger, M. Myocardial kinetics of C-11 epinephrine in the isolated working rat heart. *J. Nucl. Med.* **1997**, *38*, 780–785.
- (33) Musacchio, J. M.; Kopin, I. J.; Weise, V. K. Subcellular distribution of some sympathomimetic amines and their  $\beta$ -hydroxylated derivatives in the rat heart. *J. Pharmacol. Exp. Ther.* **1965**, *148*, 22–28.
- (34) Berry, C. R.; DeGrado, T. R.; Nutter, F.; Garg, P. K.; Breitschwerdt, E. B.; et al. Imaging of pheochromocytoma in 2 dogs using p-[<sup>18</sup>F] fluorobenzylguanidine. *Vet. Radiol. Ultrasound* **2002**, *43*, 183–186.
- (35) Berry, C. R.; Garg, P. K.; Zalutsky, M. R.; Coleman, R. E.; DeGrado, T. R. Uptake and retention kinetics of para-fluorine-18-fluorobenzylguanidine in isolated rat heart. *J. Nucl. Med.* **1996**, *37*, 2011–2016.
- (36) DeGrado, T. R.; Zalutsky, M. R.; Coleman, R. E.; Vaidyanathan, G. Effects of specific activity on meta-[<sup>123</sup>I]iodobenzylguanidine kinetics in isolated rat heart. *Nucl. Med. Biol.* **1998**, *25*, 59–64.
- (37) Raffel, D.; Loc'h, C.; Mardon, K.; Mazière, B.; Syrota, A. Kinetics of the norepinephrine analog [Br-76]-meta-bromobenzylguanidine in isolated working rat heart. *Nucl. Med. Biol.* **1998**, *25*, 1–16.
- (38) Law, M. P.; Osman, S.; Davenport, R. J.; Cunningham, V. J.; Pike, V. W.; et al. Biodistribution and metabolism of [N-methyl-<sup>11</sup>C]-m-hydroxyephedrine in the rat. *Nucl. Med. Biol.* **1997**, *24*, 417–424.
- (39) Carr, E. A.; Carroll, M.; Counsell, R. E.; Tyson, J. W. Studies of uptake of the bremelium analogue, iodobenzyltrimethylammonium iodide, by non-primate, monkey and human heart. *Br. J. Clin. Pharmacol.* **1979**, *8*, 425–432.
- (40) Dae, M. W.; De Marco, T.; Botvinick, E. H.; O'Connell, W.; Hattner, R. S.; et al. Scintigraphic assessment of MIBG uptake in globally denervated human and canine hearts – implications for clinical studies. *J. Nucl. Med.* **1992**, *33*, 1444–1450.
- (41) Glowniak, J.; Turner, F.; Gray, L.; Palac, R.; Lagunas-Solar, M.; et al. Iodine-123 metaiodobenzylguanidine imaging of the heart in idiopathic congestive cardiomyopathy and cardiac transplants. *J. Nucl. Med.* **1989**, *30*, 1182–1191.
- (42) Eisenhofer, G.; Smolich, J. J.; Esler, M. D. Disposition of endogenous adrenaline compared to noradrenaline released by cardiac sympathetic nerves in the anaesthetized dog. *Naunyn-Schmiedeberg's Arch. Pharmacol.* **1992**, *345*, 160–171.
- (43) Raffel, D. M.; Corbett, J. R.; del Rosario, R. B.; Gildersleeve, D. L.; Chiao, P. C.; et al. Clinical evaluation of carbon-11-phenylephrine: MAO sensitive marker of cardiac sympathetic neurons. *J. Nucl. Med.* **1996**, *37*, 1923–1931.
- (44) Sisson, J. C.; Shulkin, B. L. Nuclear medicine imaging of pheochromocytoma and neuroblastoma. *Q. J. Nucl. Med.* **1999**, *43*, 217–223.
- (45) Braun, C. E. Preparation of some structurally related monoguanidines. *J. Am. Chem. Soc.* **1933**, *55*, 1280–1284.
- (46) Spickett, R. G. W.; Durant, G. J.; Willey, G. L. *Guanidines*. GB 1040542, 1966.
- (47) Aroyan, A. A.; Kocharyan, S. P. Synthesis of some amines, amidoximes, and derivatives of guanidine. *Izv. Akad. Nauk Arm. SSR, Khim. Nauki* **1964**, *17*, 543–548.
- (48) Sperry, S.; Crews, P. Dihydrotrabastines: phenethylguanidine analogs from the Indo-Pacific marine sponge *Petrosia* cf. *contignata*. *J. Nat. Prod.* **1998**, *61*, 859–861.
- (49) Lee, H.; Inbasekaran, M. N.; Wieland, D. M.; Sherman, P. S.; Fisher, S. J.; et al. Development of a kit-form analog of metaiodobenzylguanidine. *J. Nucl. Med.* **1986**, *27*, 256–267.
- (50) Jewett, D. M. A simple synthesis of [<sup>11</sup>C]-methyl triflate. *Appl. Radiat. Isot.* **1992**, *43*, 1383–1385.
- (51) National Research Council. *Guide for the Care and Use of Laboratory Animals*; U.S. Department of Health and Human Services, National Institutes of Health: Bethesda, MD, 1985.
- (52) Taegtmeier, H.; Hems, R.; Krebs, H. A. Utilization of energy providing substrates in the isolated working rat heart. *Biochem. J.* **1980**, *186*, 701–711.